Pakistan J. Zool., pp 1-11, 2026. **DOI**: https://dx.doi.org/10.17582/journal.pjz/20250817161448

Mechanistic Insights into the Antiviral Potential of *Punica granatum* Phytocompounds as Inhibitors of Dengue Virus NS5 RdRp: An Integrated Computational Approach

Maham Fatima[1], Nazima Yousaf Khan[2], Tahira Bibi[3], Waqas Ahmad[4,5] and Muhammad Azeem[6]*

[1]*Department of Physiology, Faculty Life Sciences, Government College University, Faisalabad, Pakistan*
[2]*Institute of Biochemistry, University of Balochistan, Quetta, Pakistan*
[3] *Department of Botany, Sardar Bahadur Khan Women's University, Quetta, Pakistan*
[4] *Department of Pathology, University of Veterinary and Animal Sciences, Lahore, Pakistan*
[5]*Livestock and Dairy Development Department, Government of the Punjab, Lahore, Pakistan*
[6]*Department of Allied Health Sciences, Superior University, Lahore, Pakistan*

Article Information
Received 17 August 2025
Revised 10 September 2025
Accepted 29 September 2025
Available online 23 March 2026
(early access)

Authors' Contribution
MF and NYK conceived and designed the study and drafted the initial draft. TB contributed to validation of results. WA did data analysis, software application, methodology, visualization and reviewed the manuscript. MA supervised the research, provided conceptual guidance, reviewed and edited the manuscript and approved the final version.

Key words
Punica granatum, Dengue virus, RNA-dependent RNA polymerase, Phytochemicals, Molecular docking, Antiviral agents

ABSTRACT

Dengue virus is a significant arboviral pathogen of tropical regions, and it continues to lack effective targeted antiviral treatments. This study aimed to identify *Punica granatum* phytoconstituents as potential natural inhibitors of the NS5 RNA-dependent RNA polymerase (RdRp) of dengue virus using computational methods. The crystal structure of NS5 RdRp and *P. granatum* phytochemicals were used for molecular dockings, binding free energy calculations, pharmacokinetic profiling via QikProp, and molecular dynamics (MD) simulation analysis, along with post-MD/MM-GBSA analysis and principal component analysis (PCA). Dynamic cross-correlation matrix (DCCM) analysis was also performed to evaluate the stability and correlated motions of residues during the MD simulation to gain insights into correlated dynamics underlying structural integrity. Granatin B showed the strongest binding affinity (Glide XP GScore: -14.59, ΔG bind: -61.23 kcal/mol), followed by Punicalagin (GScore: -8.75, ΔG bind: -50.84 kcal/mol). ADMET predictions indicated acceptable pharmacokinetics for both compounds. The MD simulations showed stability (RMSD; 2.0–2.5 Å) for both Granatin B and punicalagin–NS5 complexes. Post-MD/MM-GBSA analysis showed higher mean binding free energies (−59.8 kcal/mol) for Granatin B–NS5 interactions (PC1 and PC2; 32%). DCCM analysis revealed stable correlation patterns across the simulation, indicating consistent inter-residue communication and structural integrity during the MD trajectory. Our findings suggest that *P. granatum* constituents, especially Granatin B, have significant potential inhibitory action against dengue NS5 RdRp.

INTRODUCTION

Dengue virus (DENV), a mosquito-borne pathogen of the Flaviviridae family, poses a serious and growing global health threat, with an estimated 390 million infections annually and up to 100 million symptomatic cases, including half a million severe illnesses per year (Thomas *et al*., 2023). The virus causes a wide spectrum of clinical outcomes, from mild febrile illness to severe dengue hemorrhagic fever and shock syndrome (Guzman and Martinez, 2024). Currently, there is no specific antiviral therapy, and vaccine use remains limited due to serotype-dependent immunity and risks of antibody-dependent enhancement (Huang *et al*., 2021). These shortcomings underscore the urgent need for effective antiviral interventions.

The nonstructural protein 5 (NS5) of DENV, the largest and most conserved protein (~900 residues) across

* Corresponding author: muhammad.azeem@superior.edu.pk
0030-9923/2026/0001-0001 $ 9.00/0

all four serotypes, functions as a bifunctional enzyme comprising an N-terminal methyltransferase (MTase) and a C-terminal RdRp (Nath *et al*., 2024). The MTase cap structures the viral RNA to facilitate replication, while the RdRp initiates and elongates the viral genome the latter featuring well-defined structural motifs critical for function, such as a right-hand architecture containing fingers, palm, and thumb subdomains and conserved motifs A–G (dos Santos Nascimento *et al*., 2021; Nath *et al*., 2024). These attributes, coupled with its essential role in viral replication and lack of a human homolog, mark NS5 RdRp as a prime drug target (dos Santos Nascimento *et al*., 2021).

Efforts to inhibit NS5 RdRp have encompassed both nucleoside inhibitors (NIs), which act as chain terminators, and non-nucleoside inhibitors (NNIs), which bind to allosteric pockets (Dos Santos Nascimento *et al*., 2021; Sreekanth, 2023). While several potent NIs have been synthesized, many exhibit high cytotoxicity or limited cellular efficacy. On the other hand, allosteric inhibitors such as NITD 434 and NITD 640 bind within the RNA template channel, inducing conformational changes that impair RdRp function (Barik, 2022). Notably, RK 0404678 has displayed *in-vitro* pan-serotype activity by engaging two conserved binding sites, yet its affinity (EC_{50} ranging from 6 µM to 46 µM across serotypes) indicates room for improvement (Quek, 2021).

Parallel to synthetic drug efforts, natural products have demonstrated promise against NS5 RdRp. A structure–activity relationship study identified biflavonoids like amentoflavone and robustaflavone as potent enzymatic inhibitors, with sotetsuflavone showing an IC_{50} of just 0.16 µM (Menezes and Campos, 2021). Additionally, plant extracts containing flavonoids and alkaloids have shown inhibitory activity, although many require additional optimization. These findings validate the potential of plant-derived compounds in DENV antiviral discovery (Akram *et al*., 2024).

Despite mounting evidence of *in vitro* efficacy, most studies lack integration of computational screening, binding energy validation, pharmacokinetic profiling, and dynamics simulation steps, which are vital for identifying viable lead compounds. In particular, *P. granatum* (pomegranate) is a rich and underexplored source of bioactive phytochemicals, yet its potential against DENV NS5 RdRp remains unexplored.

There is a lack of a comprehensive, structure-based methodology that applies docking, binding free energy, ADME evaluation, and molecular dynamics to *P. granatum* phytoconstituents targeting NS5 RdRp. Consequently, there is a scarcity of validated data to support their candidacy as antiviral leads. This study addresses a critical gap in antiviral drug discovery by retrieving and preparing the DENV NS5 RdRp structure, followed by molecular docking of *P. granatum* phytochemicals. Top-ranked compounds were further validated through post-docking MM-GBSA analysis and evaluated for pharmacokinetic properties via QikProp. To assess the dynamic stability of ligand–protein complexes, Desmond MD simulations were performed, followed by thermal MM-GBSA calculations and PCA.

MATERIALS AND METHODS

Retrieval and preparation of NS5 protein structure

The 3D crystal structure of the RdRp domain of the dengue virus NS5 protein was retrieved from the Protein Data Bank (https://www.rcsb.org/structure/5ZQK). Structural assessment was conducted via ProSA-web (https://prosa.services.came.sbg.ac.at/prosa.php), ProtParam (https://web.expasy.org/protparam/) for physicochemical parameters, and Ramachandran plot (Carugo and Djinović-Carugo, 2013) to verify stereochemical quality. The structure was refined using the Protein Preparation Wizard in Schrödinger Maestro (v2024-4), which involved assigning bond orders, adding hydrogens, optimizing hydrogen bonds, removing water molecules beyond 3Å from heteroatoms, and performing restrained energy minimization using the OPLS4 force field (Sahayarayan *et al*., 2021).

Binding site identification

Binding site prediction was carried out using SiteMap (Schrödinger) with the following criteria of Site score ≥ 1.0, Dscore ≥ 1.0. The highest-ranked site was selected for receptor grid generation for docking purposes (Murtuja *et al*., 2024).

Ligand preparation

Phytocompounds of *P. granatum* were retrieved from the Indian medicinal plants, phytochemistry and therapeutics (IMPPAT) database (https://cb.imsc.res.in/imppat/). Ligand structures were prepared using LigPrep through Epik, and pH was set at 7.0 ± 2.0 using the Ionizer module. Multiple stereoisomers and tautomers were generated (up to 32 per compound), retaining specific chirality, and energy minimization was conducted using the OPLS4 force field (Venkatesan *et al*., 2018).

Molecular docking

Molecular docking was performed using the Glide XP (Extra Precision) protocol to evaluate binding affinities and molecular interactions. The receptor grid was defined around the SiteMap-predicted active site. Standard docking

parameters included van der Waals scaling: 0.80 (for ligands), with partial charge cutoff: 0.15, flexible ligand sampling, and Epik state penalties (John *et al*., 2024). Docking performance was evaluated using GlideScore to evaluate binding affinity and calculated using the formula:

GlideScore= (0.065) × vdW + 0.130 × coul + Lipo + Hbond + Metal + BuryP + RotB + Site

where vdW is van der Waals interaction energy, Coul is electrostatic (Coulombic) energy, Lipo is lipophilic contact term, Hbond is hydrogen bonding energy, metal is metal-ligand interaction term, BuryP is penalty for buried polar groups not forming hydrogen bonds, RotB is penalty for ligand conformational flexibility (rotatable bonds), Site is reward/penalty based on binding-site interactions. Lower GlideScores represented stronger binding affinities.

ADME prediction

Drug-likeness and ADME properties were evaluated using QikProp (Schrödinger) (Hasan *et al*., 2022).

Molecular dynamics simulation

A 10 ns MD simulation was performed using Desmond to evaluate the dynamic stability of the top protein–ligand complex. The system was solvated using the TIP5P water model within an orthorhombic box, maintaining a 10 Å buffer around the complex. Sodium and chloride ions were added to neutralize the system and mimic a 0.15 M physiological saline environment. The simulation was carried out under NPT ensemble conditions, with temperature maintained at 300 K using the Nose–Hoover thermostat and pressure at 1.01325 bar regulated by the Martyna–Tobias–Klein barostat. The OPLS4 force field was applied, with trajectory frames recorded every 10 ps intervals. Simulation outputs such as root mean square deviation (RMSD), root mean square fluctuation (RMSF), protein–ligand contacts, and interaction persistence were analyzed to validate complex stability (Li *et al*., 2024).

Binding free energy calculations (MM-GBSA)

Binding free energy calculations were performed twice during the procedure. Initial MM-GBSA was performed for post-docking binding free energy estimations using Prime MM-GBSA calculations with the OPLS4 force field and the VSGB 2.1 implicit solvation model. The final calculations were performed on the frames from the output trajectory file of the MD simulation. The following equation was applied:

Δ G bind G complex = (G protein + G ligand)

where G complex is total energy of the protein-ligand complex, G protein is energy of the unbound protein, and G ligand is energy of the unbound ligand. The total energy (G) includes molecular mechanics energies (electrostatics, van der Waals), solvation energy, and surface area energy. Negative ΔG bind values indicate favorable binding (Murtuja *et al*., 2024).

Dynamics cross-correlation analysis

Dynamic cross-correlation maps (DCCMs) were computed using the Bio3D package in R to assess correlated and anti-correlated motions between residue pairs, where positive correlations were shown in red and negative correlations in blue.

Statistical analysis

Molecular dynamics simulation trajectories were generated using Desmond (Schrödinger Suite), and the output topology files were processed to extract Cα atomic coordinates. Principal component analysis (PCA) was performed in RStudio version 4.4.3 using the "Bio3d" package to evaluate the major conformational motions of the dengue virus NS5 RdRp protein in complex with *P. granatum* extract constituents (El-Daly *et al*., 2025). The first few components representing the most significant structural variations were analyzed and visualized to elucidate the dynamic effects of ligand binding.

RESULTS

Structural validations

The structure of the NS5 protein of dengue virus was obtained from the Protein Data Bank (PDB) under accession number 5ZQK. Structural analysis was performed using X-ray diffraction. The structure resolution was 2.30 Å. The analysis yielded an R-value of 0.235, an R-value work of 0.196, and an R-value of 0.198 (Fig. 1).

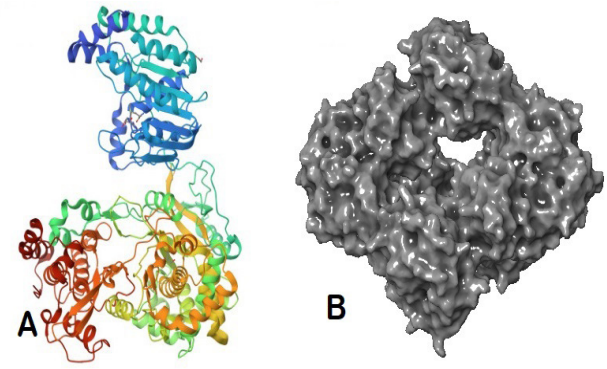

Fig. 1. (A) Ribbon representation of the 3D structure of the NS5 protein from the dengue virus displaying the intricate folding and domain organization. (B) Surface representation showing the external topology and potential interaction sites.

The structural validation of the NS5 protein of dengue virus using the ProSA web server yielded a Z-score of 10.86 and showed a high-quality structure within the range of experimentally determined protein structures. Ramachandran plot analysis via PROCHECK showed 91.9% of residues in the most favored regions, 7.5% in allowed regions, 0.0% in generously allowed regions, and only 0.6% in disallowed regions, further supporting the structural quality. The VERIFY3D analysis indicated that 87.94% of the residues had an average 3D-1D score ≥ 0.1, demonstrating good compatibility between the 3D model and its 1D sequence. ERRAT analysis returned an overall quality factor of 93.21%, reflecting a low number of errors in the structure. Additionally, PROCHECK reported minor deviations in bond lengths and angles, with a G-factor of 0.07 (Fig. 2).

Physicochemical properties and sitemap analysis

The ProtParam analysis of the NS5 protein revealed its amino acid composition, with a significant presence of Glu (8.6%) and Gly (8.2%) as the most abundant residues, followed by Leu (7.6%) and Lys and Thr (each 6.9%). Other notable residues include Arg (6.8%), Val (6.5%), and Ser (6.1%). In contrast, Cys (1.5%), Tyr (2.6%), and Phe (2.7%) are among the least represented amino acids. Moreover, Sitemap analysis in Maestro 14 identified five potential binding sites on the NS5 protein, characterized by a range of site metrics reflecting their structural and

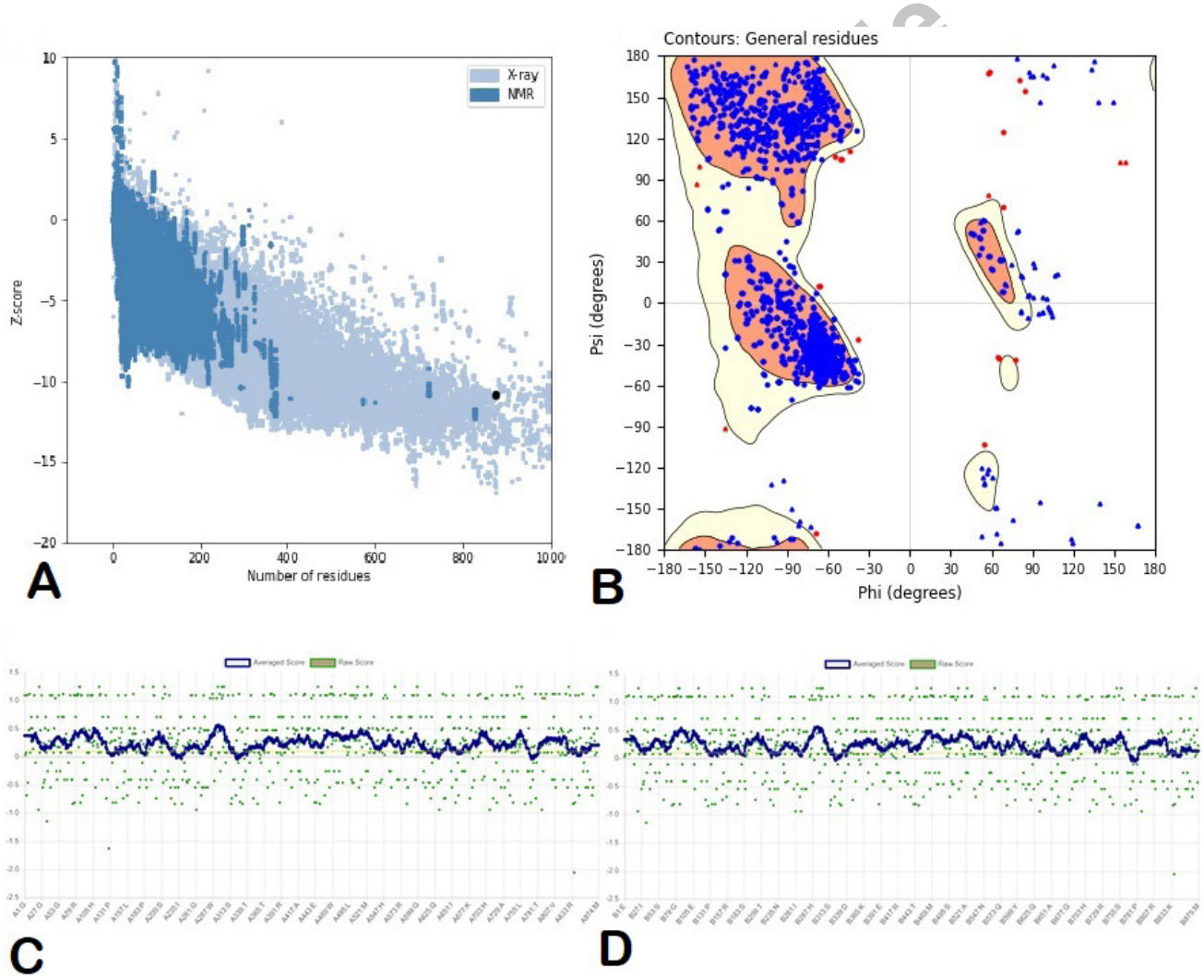

Fig. 2. Structural validation of the NS5 protein model: (A) ProSA Z-score plot showing a Z-score of -10.86, confirming model quality; (B) Ramachandran plot from PROCHECK indicating 91.9% of residues in favored regions with minimal outliers; (C) VERIFY3D assessment where 87.94% of residues scored ≥ 0.1, supporting structural reliability; (D) ERRAT quality factor of 93.21%, reflecting low error in the model.

physicochemical properties. Site 2, with a size of 424 amino acids and a D-score of 1.034, demonstrated a high site score of 1.029, indicating a well-defined binding pocket with balanced hydrophilic and hydrophobic regions (philic score: 1.075, phobic score: 0.689) and a substantial volume of 1629.1 Å³. Similarly, Site 1, comprising 494 amino acids, exhibited a D-score of 1.030 and a site score of 1.010, along with balanced hydrophobic and hydrophilic characteristics (philic score: 1.031, phobic score: 0.721) and a comparable volume of 1629.1 Å³. Site 4, although smaller with 143 amino acids and a volume of 514.5 Å³, had a site score of 1.001, suggesting a moderately defined pocket with relatively high enclosure (0.699) and exposure (1.215) scores. Site 5, with 129 amino acids, achieved the highest D-score of 1.042 and an optimal balance (balance score: 0.564) along with a volume of 475 Å³, indicating its potential as a high-affinity binding site. Lastly, Site 3, consisting of 240 amino acids, presented a moderate site score of 0.995, with lower balance (0.317) and a volume of 816.7 Å³.

Molecular dockings and post-docking MM-GBSA analysis

The molecular docking and MM-GBSA binding free energy analyses of ligands from *P. granatum* showed that Granatin B had a strong binding affinity with a Glide XP GScore of -14.59 and an Emodel score of -169.76, indicating a stable and favorable interaction within the binding pocket (Priya *et al*., 2013). Granatin B formed extensive interactions such as GLN 603, SER 601, and ASP 539, which likely stabilized the ligand within the binding site. Hydrophobic residues like ILE 797, TRP 795, and TYR 607 were also engaged, contributing to the binding through hydrophobic interactions, which further anchored the ligand in place. The presence of charged residues, including ASP 664 and GLU 459, provided additional electrostatic stabilization, while polar residues such as SER 710 and ARG 729 formed supplementary hydrogen bonds, ensuring a strong attachment of Granatin B within the pocket. Punicalagin also established numerous hydrogen bonds with residues like ASP 664, SER 661, and GLU 459, which were crucial for ligand stabilization. Additional interactions with polar residues, including LYS 461 and ARG 472, further enhanced binding affinity. Punicalagin also formed hydrophobic interactions with residues such as TRP 475 and ILE 414, which contributed to the non-polar stabilization of the ligand in the hydrophobic regions of the active site. Charged residues like ASP 539 and GLY 537 formed salt bridges, adding electrostatic attraction to the binding profile (Fig. 3).

The post-docking MM-GBSA binding free energy (ΔG bind) for Granatin B was calculated as -61.23 kcal/mol, with a non-specific binding energy (ΔG bind(NS)) of -99.57 kcal/mol. This binding energy was characterized by significant electrostatic (Coulomb) contributions at -244.47 kcal/mol and van der Waals (vdW) interactions at -76.06 kcal/mol, as well as solvation effects with a favorable desolvation energy of 247.67 kcal/mol. Additionally, the hydrogen bonding energy contribution was calculated at -6.98 kcal/mol. Punicalagin also exhibited a favorable binding profile, with a Glide XP GScore of -8.75 and an Emodel score of -118.16. Its MM-GBSA binding free energy was -50.84 kcal/mol, with a non-specific binding energy of -81.92 kcal/mol. The binding energy of Punicalagin was supported by a Coulomb contribution of -88.83 kcal/mol, indicating moderate electrostatic interactions, and a vdW interaction of -67.81 kcal/mol, reflecting adequate hydrophobic interactions with the NS5 protein. The solvation effect provided a desolvation energy of 98.15 kcal/mol, while the hydrogen bonding component contributed -8.39 kcal/mol.

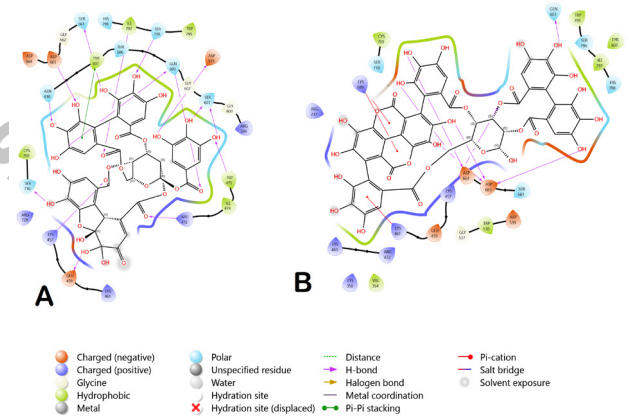

Fig. 3. Binding interactions of (A) Granatin B and (B) Punicalagin with the NS5 protein active site, showing hydrogen bonds, salt bridges, and hydrophobic interactions with key amino acid residues.

ADMET predictions

The ADMET predictions for Granatin B and Punicalagin were analyzed using QikProp to assess their pharmacokinetic and physicochemical properties. Granatin B demonstrated a FISA value of 749.545, slightly higher than Punicalagin's 744.94, suggesting a marginal difference in lipophilicity. In terms of PISA, Granatin B (174.407) showed slightly lower polarity compared to Punicalagin (172.881), indicating that both compounds have similar polarities. The PSA (polar surface area) for both compounds, Granatin B (479.915) and Punicalagin (522.377), was within the range indicating good bioavailability, though Granatin B had a lower value, which may correlate with better cellular permeability.

The QPlogBB values, indicating blood-brain barrier penetration, were both highly negative, with Granatin B (-8.239) and Punicalagin (-8.212), suggesting poor central nervous system penetration for both compounds. The QPlogHERG values for Granatin B (-5.625) and Punicalagin (-5.217) were within a similar range, reflecting a low likelihood of arrhythmogenic effects. For the skin permeability parameter (QPlogKp), Granatin B (-13.183) and Punicalagin (-12.335) both exhibited very low values, indicating poor skin permeability. The QPlogPo/w values, which reflect the compounds' lipophilicity, were also negative for both, with Granatin B (-4.133) and Punicalagin (-4.914), reinforcing the compounds' moderate lipophilic nature. The QPlogS values for both compounds were negative, with Granatin B (-3.163) showing slightly better solubility compared to Punicalagin (-1.263). Both compounds displayed a relatively low SASA (solvent accessible surface area), with Granatin B (69.544) and Punicalagin (68.884). The dipole moments of Granatin B (995.299) and Punicalagin (999.411) were comparable, suggesting similar polar characteristics. Finally, Granatin B had a slightly lower molecular weight (952.656) compared to Punicalagin (1084.731) (Table I).

Table I. ADMET predictions for Granatin B and Punicalagin, including key pharmacokinetic and physicochemical parameters such as FISA, PISA, PSA, QPlogBB, QPlogHERG, QPlogKp, QPlogPo/w, QPlogS, QPpolrz, SASA, dipole moment, and molecular weight.

Title	FISA	PISA	PSA	QPlogBB	QPlogH-ERG	QPlog-Kp	QPlog-Po/w	QPlogS	QP polrz	SASA	dipole	mol MW
Granatin B	749.545	174.407	479.915	-8.239	-5.625	-13.183	-4.133	-3.163	69.544	995.299	15.738	952.656
Punicalagin	744.94	172.881	522.377	-8.212	-5.217	-12.335	-4.914	-1.263	68.884	999.411	10.719	1084.731

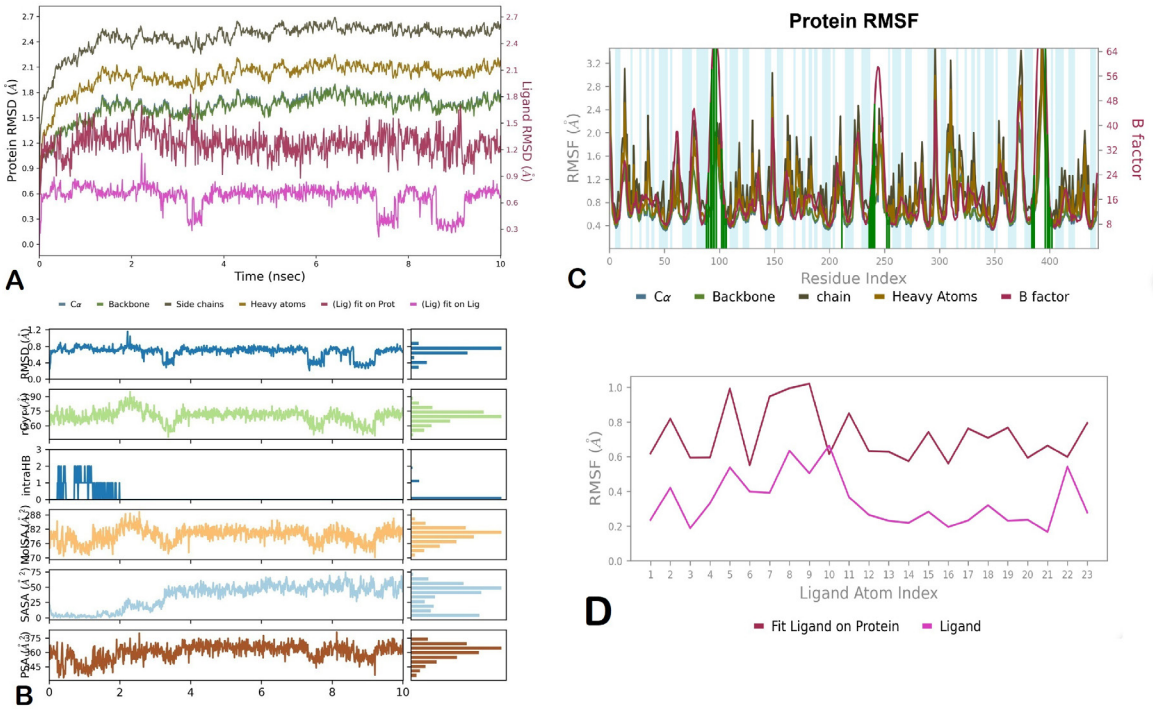

Fig. 4. (A) RMSD plots of protein Cα atoms, backbone, side chains, and heavy atoms, along with ligand RMSD (lig-fit-protein and lig-fit-ligand), showing structural stability of the protein-ligand complex over a 10 ns simulation. (B) Timeline representation of protein-ligand interactions (e.g., hydrogen bonds, hydrophobic contacts, and water bridges) across key residues, indicating persistent and stable binding throughout the simulation. (C) Root mean square fluctuation (RMSF) of protein residues showing flexibility profiles of Cα atoms, backbone, side chains, and heavy atoms over the simulation. The B-factor is overlaid for comparison. Peaks indicate regions of high mobility, while shaded regions highlight secondary structure elements. (D) Ligand RMSF plotted per atom index, comparing fluctuations when the ligand is fit on the protein versus when fit on the ligand itself.

Molecular dynamics simulation analysis

The results of MD simulation of the protein-ligand complex revealed that the Cα atoms, backbone, and heavy atoms exhibited stable fluctuations throughout the simulation RMSD <2.0 Å. The ligand RMSD also remained consistently below 1.0 Å. The interaction timeline analysis revealed persistent interactions, including hydrogen bonds, hydrophobic contacts, and water bridges, throughout the simulation time. Notably, no significant intramolecular hydrogen bonding within the ligand was observed (Fig. 4).

Post-molecular dynamics simulation MM/GBSA and dynamics cross-correlation analysis

The trajectory-based thermal MM-GBSA results showed strong agreement with the post-docking MM-GBSA binding energies, supporting the stability and consistency of ligand–protein interactions during molecular dynamics simulations. Granatin B exhibited an average binding free energy of -59.8 kcal/mol, while Punicalagin showed a comparable thermal MM-GBSA ΔG of -49.5 kcal/mol. Both ligands demonstrated favorable van der Waals and Coulombic contributions, with moderate desolvation penalties, indicating energetically stable and specific binding. The ligand strain energies remained within acceptable limits, and ligand efficiency values (~-0.35) (Table II).

Table II. Summary of post-dynamic simulation thermal MM-GBSA energy components for Granatin B and Punicalagin. Values represent average binding free energy (ΔG bind) and contributing interaction energies (kcal/mol) computed across the molecular dynamics trajectory.

Parameter	Granatin B (kcal/mol)	Punicalagin (kcal/mol)
dG bind	-59.8	-49.5
dG bind Coulomb	-230.5	-85.7
dG bind Hbond	-7.4	-8.1
dG bind Lipo	-14.8	-13.2
dG bind Packing	-6.2	-4.5
dG bind SelfCont	-1.0	-0.8
dG bind Solv GB	238.9	92.3
dG bind Solv SA	-5.2	-3.8
dG bind vdW	-72.5	-66.4
Lig strain energy	5.8	7.1
Rec strain energy	2.6	3.4
Prime ligand efficiency	-0.35	-0.30

Principal component analysis (PCA) revealed the clustering of conformational states along PC1 (22.13%), PC2 (10.32%), and PC3 (7.5). The scree plot confirms that the first few principal components capture a majority of the variance (PC1–PC5 account for ~69% cumulative variance). The dynamic cross-correlation map (DCCM) revealed distinct patterns of correlated (red) and anti-correlated (blue) motions among residues, indicating that the N-terminal region exhibits strong positive correlations, while several long-range anti-correlated interactions are observed between the central and C-terminal domains, suggesting coordinated but opposing domain motions contributing to the protein's functional dynamics (Fig. 5).

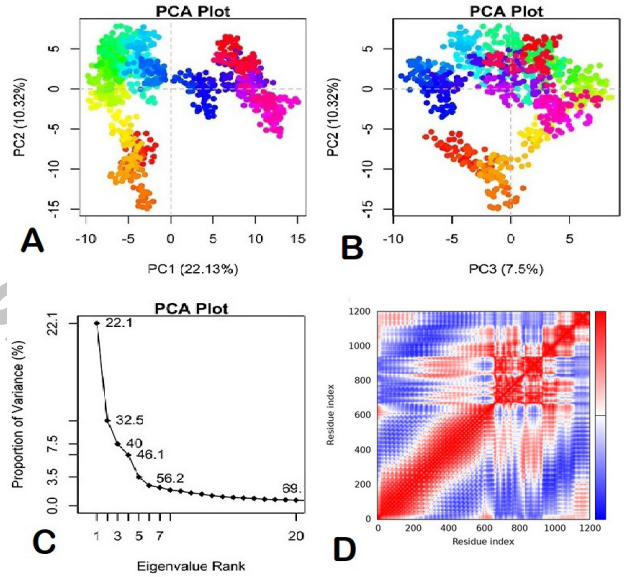

Fig. 5. PCA and DCCM analyses of the molecular dynamics trajectories. (A) Projection of the first two principal components (PC1 vs. PC2), showing conformational clustering. (B) Projection of PC2 vs. PC3, highlighting additional conformational transitions. (C) Scree plot representing the eigenvalue rank against the proportion of variance, indicating that the first few components capture the majority of the system's motions. (D) DCCM plot illustrating residue–residue correlations, where red indicates positive correlation and blue indicates negative correlation between atomic fluctuations.

DISCUSSION

In this study, we employed an integrated structure-based approach to evaluate the antiviral potential of *P. granatum* phytochemicals against the RdRp domain of dengue virus NS5. Our computational pipeline, comprising protein preparation, docking, ADMET

profiling, MD simulations, and MM-GBSA binding free energy calculations, identified Granatin B and Punicalagin as the most promising inhibitors. Granatin B exhibited the highest binding affinity (Glide XP GScore = -14.59) and most favorable MM-GBSA ΔG bind of -61.23 kcal/mol, driven primarily by strong electrostatic (-244.47 kcal/mol) and van der Waals (-76.06 kcal/mol) interactions. These values exceed those typically reported for flavonoid-like inhibitors against NS5 (e.g., flavonoid docking scores = -8 to -10, ΔG bind ≈ -35 to -50 kcal/mol), indicating good target engagement (Jonghe *et al*., 2021; Rani *et al*., 2024).

Our results align with a recent *in-silico* study on pomegranate-derived compounds, where Punicalagin demonstrated binding affinity of −6.39 kcal/mol against DENV-3 NS5, outperforming ribavirin control (Kautsar *et al*., 2024). However, they did not further validate the model through MD simulations and post-MD simulation analysis. Moreover, Granatin B was reported against influenza, EV71, and HSV-1 (Lalani and Poh, 2020; El-Aguel *et al*., 2022; Alexova *et al*., 2023). The key binding residues, including GLN603, ASP539, and TRP795, were consistently engaged through hydrogen bonds, electrostatic, and hydrophobic interactions. These residues fall within functionally conserved motifs (A–G) of NS5 RdRp that govern polymerase activity (e.g., motif C ASP538), positioning these compounds to effectively disrupt RdRp catalysis (Dos Santos Nascimento *et al*., 2021). Our findings complement existing MD and docking studies of flavonoids targeting NS5 and NS3, which demonstrate the centrality of similar residues for inhibitory action (Qamar *et al*., 2017; Yadav *et al*., 2021; Hossain *et al*., 2025).

From an ADMET perspective, both ligands exhibited low CNS penetration (QPlogBB ≈ -8.2), favorable solubility (QPlogS = -3.16 for Granatin B), acceptable lipophilicity, and no violations of Lipinski's rules aside from high molecular weight (Alghamdi *et al*., 2022). These properties suggest a promising pharmacokinetic profile for an antiviral targeting a peripheral infection. Their physicochemical properties are comparable to or better than those observed for other natural antiviral leads in NS5 studies, which often face solubility and absorption challenges (Papaya leaf flavonoids; Demonstrated by Kaempferol and Quercetin) (Senthilvel *et al*., 2013; Madushanka *et al*., 2022; Saptarini *et al*., 2024).

Notably, the MD simulation confirmed the kinetic stability of the top-ranking protein–ligand complex (Granatin B–NS5). The complex maintained RMSD fluctuations within 2.5 Å after an initial equilibration phase, and hydrogen bond persistence was high, with key residue interactions sustained throughout the trajectory. This dynamic stability aligns with reports from MD investigations of NS5 ligand pairs, where stable RMSD and consistent residue engagement were associated with functional inhibition (Reddy, 2011). Such dynamical validation bolsters the predictive value of docking and end-state energy assessments.

While our findings strongly support the antiviral potential of *P. granatum*-derived compounds against DENV NS5 RdRp, the translational value of these results hinges on future experimental substantiation. The integration of *in-vitro* enzymatic inhibition assays, cell-based antiviral studies, and *in-vivo* efficacy models will be critical in confirming the biological activity of Granatin B and Punicalagin (Akpinar-Bayizit *et al*., 2012). Moreover, structure–activity relationship (SAR) analyses and analog design could further refine binding affinity, optimize pharmacokinetics, and reduce molecular weight constraints to improve drug-likeness. Recent successes in natural product-derived antivirals, such as baicalin derivatives for SARS-CoV-2 RdRp and epigallocatechin gallate analogs in HCV inhibition, underscore the promise of this approach when paired with empirical validation (Chapman and Andurkar, 2022).

Despite these promising results, our study remains purely computational. As with similar studies, the key limitations include the absence of experimental validation and potential challenges related to oral druggability, particularly given Granatin B's large molecular weight (~952 g/mol). Future work should include in vitro enzyme assays to confirm RdRp inhibition and cellular antiviral efficacy against dengue virus serotypes, as well as potency assays. Additionally, lead optimization to reduce molecular size or enhance blood–brain barrier exclusion could improve drug-like properties (Trippier, 2016). Extending MD simulations beyond 50 ns would further clarify binding dynamics and escape pathways *in-silico* (Weng *et al*., 2021).

Hence, this study lays a rational foundation for targeted experimental research on pomegranate phytochemicals, contributing to the expanding landscape of phytochemical-driven antiviral discovery against neglected tropical diseases, such as dengue. Taken together, our integrated computational study underscores the therapeutic potential of pomegranate-derived ellagitannins, especially Granatin B, as novel inhibitors of dengue NS5 RdRp. Strong binding, favorable energetics, and kinetic stability support prioritizing these compounds for experimental validation.

CONCLUSIONS

This study successfully identified Granatin B and Punicalagin as promising natural inhibitors of the NS5 RdRp of dengue virus, two phytoconstituents from

P. granatum. Granatin B exhibited a superior binding affinity. The findings suggest that, particularly Granatin B, warrants further experimental validation as a potential lead in dengue antiviral drugs.

DECLARATIONS

Funding

This research received no external funding.

Ethical approval

Not applicable.

Data availability

All data is available in the manuscript.

Generative AI and AI-assisted technology statement

The authors declare that no generative AI and AI assisted technology was used in the creation of this manuscript.

Statement of conflict of interest

The authors have declared no conflict of interest.

REFERENCES

Akpinar-Bayizit, A., Ozcan, T. and Yilmaz-Ersan, L., 2012. The therapeutic potential of pomegranate and its products for prevention of cancer. *W: AG Georgakilas (red.), Cancer Prevent. From Mechan. Transl. Benef.*, **20**: 331-373. https://doi.org/10.5772/30464

Akram, M., Hameed, S., Hassan, A. and Khan, K.M., 2024. Development in the inhibition of dengue proteases as drug targets. *Curr. med. Chem.*, **31**: 2195-2233. https://doi.org/10.2174/0929867331666230918110144

Alexova, R., Alexandrova, S., Dragomanova, S., Kalfin, R., Solak, A., Mehan, S., Petralia, M.C., Fagone, P., Mangano, K. and Nicoletti, F., 2023. Anti-COVID-19 potential of ellagic acid and polyphenols of *Punica granatum* L. *Molecules*, **28**: 3772. https://doi.org/10.3390/molecules28093772

Alghamdi, S.S., Suliman, R.S., Aljammaz, N.A., Kahtani, K.M., Aljatli, D.A. and Albadrani, G.M., 2022. Natural products as novel neuroprotective agents; computational predictions of the molecular targets, ADME properties, and safety profile. *Plants*, **11**: 549. https://doi.org/10.3390/plants11040549

Barik, S., 2022. Inhibition of viral RNA-dependent RNA polymerases by nucleoside inhibitors: An illustration of the unity and diversity of mechanisms. *Int. J. mol. Sci.*, **23**: 12649. https://doi.org/10.3390/ijms232012649

Carugo, O. and Djinović-Carugo, K., 2013. Half a century of Ramachandran plots. *Biol. Crystallogr.*, **69**: 1333-1341. https://doi.org/10.1107/S090744491301158X

Chapman, R.L. and Andurkar, S.V., 2022. A review of natural products, their effects on SARS-CoV-2 and their utility as lead compounds in the discovery of drugs for the treatment of COVID-19. *Med. Chem. Res.*, **31**: 40-51. https://doi.org/10.1007/s00044-021-02826-2

Dos Santos Nascimento, I.J., da Silva Santos-Junior, P.F., de Aquino, T.M., de Araujo-Junior, J.X. and da Silva-Junior, E.F., 2021. Insights on Dengue and Zika NS5 RNA-dependent RNA polymerase (RdRp) inhibitors. *Eur. J. med. Chem.*, **224**: 113698. https://doi.org/10.1016/j.ejmech.2021.113698

El-Aguel, A., Pennisi, R., Smeriglio, A., Kallel, I., Tamburello, M.P., D'Arrigo, M., Barreca, D., Gargouri, A., Trombetta, D. and Mandalari, G., 2022. Punica granatum peel and leaf extracts as promising strategies for HSV-1 treatment. *Viruses*, **14**: 2639. https://doi.org/10.3390/v14122639

El-Daly, M.M., Bajrai, L.H., Alandijany, T.A., Alsaady, I.M., Gattan, H.S., Alhamdan, M.M., Dwivedi, V.D. and Azhar, E.I., 2025. Exploring Echinacea angustifolia for antiviral compounds against Zika virus RNA-dependent RNA polymerase: A computational study. *Sci. Rep.*, **15**: 4060. https://doi.org/10.1038/s41598-025-88481-8

Guzman, M.G. and Martinez, E., 2024. Central and peripheral nervous system manifestations associated with dengue illness. *Viruses*, **16**: 1367. https://doi.org/10.3390/v16091367

Hasan, M.M., Khan, Z., Chowdhury, M.S., Khan, M.A., Moni, M.A. and Rahman, M.H., 2022. *In silico* molecular docking and ADME/T analysis of Quercetin compound with its evaluation of broad-spectrum therapeutic potential against particular diseases. *Inf. Med. Unlock.*, **29**: 100894. https://doi.org/10.1016/j.imu.2022.100894

Hossain, A., Joti, F.T., Hossain, M.S., Al-Noman, A., Thowing, C., Mursona, M., Islam, M.R., Rahman, M.E., Matin, M.N. and Haque, M.A., 2025. Identification of potential inhibitors targeting nonstructural proteins NS3 and NS5 of dengue virus using docking and deep learning approaches. *Pharmaceuticals*, **18**: 566. https://doi.org/10.3390/ph18040566

Huang, C.-H., Tsai, Y.-T., Wang, S.-F., Wang, W.-H. and Chen, Y.-H., 2021. Dengue vaccine: An update.

Expert Rev. Anti Infect. Ther., **19**: 1495-1502. https://doi.org/10.1080/14787210.2021.1949983

John, A.M., Suresh, S.C., Baby, A., Jayaram, S., Sarojini, S., Thomas, R. and Balakrishnan, S.P., 2024. Unveiling the therapeutic potential of azopyridine derivatives for trypsin inhibition: A DFT and *in-vitro* approach. *Mol. Physiol.*, pp. e2415951. https://doi.org/10.1080/00268976.2024.2415951

Jonghe, D.J., Neyts, J., Kowalska, J., Jemielity, J., Vangeel, L. and Jonghe, S.D., 2021. Identification and evaluation of potential SARS-CoV-2 antiviral agents targeting mRNA Cap guanine N7-methyltransferase. *Antiviral Res.,* **193**: 105142. https://doi.org/10.1016/j.antiviral.2021.105142

Kautsar, R., Rachmawati, Y., Rokhim, S., Sucipto, T.H., Damayanti, M. and Ramadhani, A.H., 2024. In silico analysis of inhibitor potential of punicalagin compound in pomegranate (*Punica granatum*) against NS5 DENV-3 protein. *Indones. J. Trop. Infect. Dis.*, **12**: 24. https://doi.org/10.20473/ijtid.v12i1.52320

Lalani, S. and Poh, C.L., 2020. Flavonoids as antiviral agents for enterovirus A71 (EV-A71). *Viruses*, **12**: 184. https://doi.org/10.3390/v12020184

Li, D.D., Ma, J.R., Huang, Q.R., Man, R.J. and Zhao, L., 2024. Exploring protein-berberine interactions via molecular dynamics and MM/GBSA calculations. *J. mol. Liq.*, **411**: 125755. https://doi.org/10.1016/j.molliq.2024.125755

Madushanka, A., Verma, N., Freindorf, M. and Kraka, E., 2022. Papaya leaf extracts as potential dengue treatment: An *in-silico* study. *Int. J. mol. Sci.*, **23**: 12310. https://doi.org/10.3390/ijms232012310

Menezes, J.C. and Campos, V.R., 2021. Natural biflavonoids as potential therapeutic agents against microbial diseases. *Sci. Total Environ.*, **769**: 145168. https://doi.org/10.1016/j.scitotenv.2021.145168

Murtuja, S., Siddique, M.U.M., Shrivastava, K.P., Agarwal, Y.O., Wagh, S., Yasmin, S., Ansari, A., Shaikh, M.S., Hasnain, M.S. and Goyal, S.N., 2024. Identifying novel inhibitors for dengue NS2B-NS3 protease by combining topological similarity, molecular dynamics, MMGBSA and sitemap analysis. *Curr. Comput. Aided Drug Des.,* https://doi.org/10.2174/0115734099329789240905141013

Nath, S., Malakar, P., Biswas, B., Das, S., Sabnam, N., Nandi, S. and Samadder, A., 2024. Exploring the targets of dengue virus and designs of potential inhibitors. *Combinat. Chem. High Throug. Screen.*, **27**: 2485-2524. https://doi.org/10.2174/0113862073246789231030153054

Priya, S.S.L., Devi, P.R. and Madeswaran, A., 2013. *In silico* docking studies of RP2 (X-Linked retinitis pigmentosa) protein using anthocyanins as potential inhibitors. *Bangladesh J. Pharmacol.*, **8**: 292-299. https://doi.org/10.3329/bjp.v8i3.15110

Quek, J.P., 2021. *Understanding the molecular basis of flavivirus replication process for antiviral therapeutics development.* PhD thesis. Lee Kong Chian School of Medicine, Nanyang Technological University, Singapore.

Rani, R., Bhutkar, M. and Tomar, S., 2024. *Therapeutic antiviral potential of flavonoids*. Apple Academic Press. https://doi.org/10.1201/9781003412441-4

Reddy, T., 2011. *Structure, flexibility, and overall motion of transmembrane peptides studied by NMR spectroscopy and molecular dynamics simulations*. Ph.D thesis, Dalhousie University.

Sahayarayan, J.J., Rajan, K.S., Vidhyavathi, R., Nachiappan, M., Prabhu, D., Alfarraj, S., Arokiyaraj, S. and Daniel, A.N., 2021. *In-silico* protein-ligand docking studies against the estrogen protein of breast cancer using pharmacophore based virtual screening approaches. *Saudi J. biol. Sci.*, **28**: 400-407. https://doi.org/10.1016/j.sjbs.2020.10.023

Saptarini, N.M., Kelutur, F.J. and Corpuz, M.J.-A.T., 2024. Exploring the antidiarrheal properties of papaya leaf: Insights *in vivo* study in mic model and *in silico* analysis at M3 muscarinic acetylcholine receptor interaction. *Scientifica*, **2024**: 1558620. https://doi.org/10.1155/2024/1558620

Senthilvel, P., Lavanya, P., Kumar, K.M., Swetha, R., Anitha, P., Bag, S., Sarveswari, S., Vijayakumar, V., Ramaiah, S. and Anbarasu, A., 2013. Flavonoid from Carica papaya inhibits NS2B-NS3 protease and prevents Dengue 2 viral assembly. *Bioinformation*, **9**: 889. https://doi.org/10.6026/97320630009889

Sreekanth, G.P., 2023. Perspectives on the current antiviral developments towards RNA-dependent RNA polymerase (RdRp) and methyltransferase (MTase) domains of dengue virus nonstructural protein 5 (DENV-NS5). *Eur. J. med. Chem.*, **256**: 115416. https://doi.org/10.1016/j.ejmech.2023.115416

Thomas, S.J., Endy, T.P. and Rothman, A.L., 2023. *Flaviviruses: dengue*. Springer. https://doi.org/10.1007/978-1-4939-9544-8_15-1

Trippier, C.P., 2016. Selecting good drug-like properties to optimize small molecule blood-brain barrier penetration. *Curr. med. Chem.*, **23**: 1392-1407. https://doi.org/10.2174/0929867323666616040511

2353

Qamar, M.T., Ashfaq, U.A., Tusleem, K., Mumtaz, A., Tariq, Q., Goheer, A. and Ahmed, B., 2017. *In-silico* identification and evaluation of plant flavonoids as dengue NS2B/NS3 protease inhibitors using molecular docking and simulation approach. *Pak. J. Pharm. Sci.*, **30**: 2119-2138.

Venkatesan, A., Rambabu, M., Jayanthi, S. and Febin Prabhu Dass, J., 2018. Pharmacophore feature prediction and molecular docking approach to identify novel anti-HCV protease inhibitors. *J. Cell. Biochem.*, **119**: 960-966. https://doi.org/10.1002/jcb.26262

Weng, Y.L., Naik, S.R., Dingelstad, N., Lugo, M.R., Kalyaanamoorthy, S. and Ganesan, A., 2021. Molecular dynamics and *in silico* mutagenesis on the reversible inhibitor-bound SARS-CoV-2 main protease complexes reveal the role of lateral pocket in enhancing the ligand affinity. *Sci. Rep.*, **11**: 7429. https://doi.org/10.1038/s41598-021-86471-0

Yadav, R., Selvaraj, C., Aarthy, M., Kumar, P., Kumar, A., Singh, S.K. and Giri, R., 2021. Investigating into the molecular interactions of flavonoids targeting NS2B-NS3 protease from ZIKA virus through *in-silico* approaches. *J. Biomol. Struct. Dyn.*, **39**: 272-284. https://doi.org/10.1080/07391102.2019.1709546